International Journal of Biological Macromolecules 146 (2020) 560–568

Contents lists available at ScienceDirect

International Journal of Biological Macromolecules

journal homepage: http://www.elsevier.com/locate/ijbiomac

Chitosan mediated gold nanoparticles against pathogenic bacteria, fungal strains and MCF-7 cancer cells

R. Kalaivani [a,1], M. Maruthupandy [a,b,*,1], T. Muneeswaran [a,b,1], Manoj Singh [a,d], S. Sureshkumar [c], M. Anand [a], C.M. Ramakritinan [a], F. Quero [b], A.K. Kumaraguru [a]

[a] Department of Marine and Coastal Studies, School of Energy, Environment and Natural Resources, Madurai Kamaraj University, Madurai 625 021, Tamil Nadu, India
[b] Laboratorio de Nanocelulosa y Biomateriales, Departamento de Ingeniería Química, Biotecnología y Materiales, Facultad de Ciencias Físicas y Matemáticas, Universidad de Chile, Avenida Beauchef 851, Santiago, Chile
[c] Department of Microbial Technology, School of Biological Sciences, Madurai Kamaraj University, Madurai 625 021, Tamil Nadu, India
[d] Department of Biotechnology, Maharishi Markendeswar University, Mullana-Ambala 133-207, Haryana, Inida

ARTICLE INFO

Article history:
Received 3 June 2019
Received in revised form 17 December 2019
Accepted 5 January 2020
Available online 7 January 2020

ABSTRACT

In the present study, we report cytotoxic and antimicrobial potential of gold nanoparticles (Au NPs) synthesized using chitosan derived from squilla shell wastes. Here we adopted ecofriendly approach for the synthesis of Au NPs and characterized them using UV–visible spectroscopy, Fourier transform infrared spectroscopy, X-ray diffraction, atomic force microscopy, transmission electron microscopy (TEM) and dynamic light scattering (DLS) methods. The UV–visible spectroscopic analysis revealed an absorption peak at 529 nm, which represents the Surface Plasmon Resonance of Au NPs. TEM analysis showed that the biosynthesized Au NPs were spherical in shape with an average size of 80 to 82 nm. Interestingly, the biosynthesized Au NPs showed antimicrobial activity against selected Gram-positive and negative bacterial isolates and also showed activity against fungal pathogens. Further, the cytotoxic effect of the synthesized Au NPs against MCF-7 cell lines was assessed by MTT assay with IC50 value of 250 μg mL^{-1}. In addition, double staining of treated MCF-7 cells with acridine orange and ethidium bromide shows that the Au NPs exert apoptosis mediated cytotoxicity.

1. Introduction

Nanotechnology is an emerging field, which has potential applications in various fields, and it is generally used for the improvement of human beings' quality of life. Nanoparticles (NPs) have wide range of applications owing to their unique physical, chemical, electrical, mechanical, magnetic, thermal, dielectric, optical and biological properties [1]. Particularly, the noble metal NPs such as gold, silver and platinum are widely used in cosmetics and biomedicine. Among numerous noble metals, gold is one of the most commonly studied metal owing to its stable chemical property, biocompatibility and non-immunogenicity [2]. In particular, gold has been used in the treatment of rheumatoid arthritis [3,4]. Gold is easily formulated in various shapes and different sizes such as nanoparticles, nanorods, nanowires, nanocages and nanoclusters [5]. These fascinating aspects make gold nanoconstructs key materials of nanoscience and nanotechnology [2]. Similarly, red colloidal gold is used as revitalizer in China and India and has broad biological activity [6]. Furthermore, gold-based NPs are excellent candidate for bio-conjugation based applications [7]. Au NPs has received greater attention due to their unique and tunable surface plasmon resonance (SPR) and potential applications in biomedical science such as drug delivery [8], radiotherapy imaging [9] and gene delivery systems [10]. Besides, Au NPs exhibit size and shape dependent antimicrobial activity [11] and are promising therapeutic candidates for cancer therapy. The anticancer activity of Au NPs has been evaluated against various human cancer cells [12,13]. In addition, Au NPs have long life-time fluorescence, large two-photon excitation, high emission rate, and large Stokes shift. The mechanism of photoluminescence and photophysical properties of Au NPs is still not clearly understood. However, their unique optical properties establish Au NPs to be a novel fluorophore for a wide range of biomedical applications such as biodetection, biosensing and bioimaging in vitro and in vivo [1,14,15].

Generally, metal nanoparticles are synthesized and stabilized by chemical methods [14] (Ishida et al., 2016), electrochemical reduction [15], photochemical reactions [16], thermal decomposition [17] and also by physical methods for example heat evaporation [18]. The NPs synthesized via chemical and physical methods are highly reactive, hazardous and cause potential damage to environment [19,20]. Therefore,

* Corresponding author at: Department of Marine and Coastal Studies, School of Energy, Environment and Natural Resources, Madurai Kamaraj University, Madurai 625 021, Tamil Nadu, India.
E-mail address: mmaruthupandy@yahoo.in (M. Maruthupandy).
[1] Authors with equal contribution.

https://doi.org/10.1016/j.ijbiomac.2020.01.037
0141-8130/

there is a growing need for eco-friendly biomimetic approach for the synthesis of NPs.

Biomimetic is an interdisciplinary approach in which NPs are synthesized biologically [21]. A wide variety of biological sources such as plant extracts, microorganisms, enzymes, starch and biopolymers have been utilized by researchers towards greener synthesis of NPs. Recently, synthesis of NPs using marine resources has gained much attention [22]. However, most of marine resources have been extensively exploited for various applications and the development of nanoscience in utilizing marine resources is still at its infancy. Various marine flora, fauna and bioactive materials were used for the synthesis of NPs. Particularly, biocompatible and biodegradable sources such as seashells, pearls and fish bones have been used extensively [23].

The synthesized metal NPs can be stabilized using biopolymers to avoid particle agglomeration. Among the biopolymers, chitin/chitosan have been used extensively. Chitin is the second most naturally available biopolymer next to cellulose. Chitosan is a deacetylated chitin preferred mostly for the preparation of nanocomposite, owing to its ability to interact with metal nanoparticles [24–27]. Other natural polymers such as natural rubber [28] (Valdés et al., 2014), polysaccharides [29], cellulose [30] and starch [31] have also been used as stabilizers for the preparation of metal nanoparticles because of their biocompatibility, biodegradability and low toxicity.

Chitin is typically found as crystalline form in the exoskeleton of arthropods or in the cell walls of fungi and yeast [32]. Furthermore, marine crab and squilla exoskeleton wastes have been reported to be the most abundant sources of chitosan [33]. Nearly 60,000 tons of head and shell wastes are disposed yearly from crustacean processing industries, particularly abundant in the Gulf of Mannar Region [34]. The utilization of squilla shell (crustacean) wastes has significant ecological benefits, which could serve as an alternative to the disposal of crustacean wastes.

The main objective of our work is to utilize squilla shell waste for the synthesis of Au NPs. We have previously reported the synthesis of chitosan nanoparticle from crab and squilla waste [35]. In the present study, we describe the synthesis, characterization and cytotoxic effects of Au NPs derived from squilla shell wastes, which could be exploited in the near future for therapeutic applications.

2. Materials and method

2.1. Collection of squilla shell waste

Squilla mantis shells were collected from local fishermen of Mandapam Coast, Ramnad district Tamil Nadu. The species were selected based on the biological richness and availability in the Gulf of Mannar Region. The samples were washed to remove the epiphytes, sediments etc. The shells were separated, washed with distilled water and dried at room temperature in a dust free environment for two weeks. The dried shells were grounded and sieved using 0.3–0.5 mm mesh. The final yield was determined by physical measurement and subjected to chitin extraction. The chitin was further processed with the demineralization (DM), deproteinization (DP), decolorization (DC), deacetylation (DA) for the production of chitosan and the extracted chitosan as well as its characrerization was reported in our previous article [33]. Finally, the obtained chitosan was used to carry out a biological synthesis of Au NPs (Scheme 1).

2.2. Chitosan mediated Au NPs

Nearly 0.25 g of extracted chitosan was dissolved in 10 ml of 1% acetic acid followed by stirring for 30 min. Due to the poor solubility of chitosan, the mixture was vortexed and then filtered with Whatman No. 1 filter paper to obtain clear solution, which was stored for about a week until further use. This solution served as stock and was diluted to the needed concentrations. An aqueous solution of 1 mM $HAuCl_4$ (gold chloride; 1 mL) was mixed with chitosan solution (3 mL), and then the mixture was heated up to 70 °C in water bath under magnetic stirring until a red solution was obtained [36]. The change of color of the solution occured from colorless to ruby red color, indicating the formation of Au NPs. Simultaneously, a control setup was maintained without adding $HAuCl_4$. The synthesized NPs-containing solutions were centrifuged thrice at 3000 rpm for 30 min using a refrigerated centrifuge (REMI, India). The pellets were collected and dispersed in sterile deionised water. The purified particles were freeze-dried using a freeze dryer (Micro Modulyo 230, Thermo Electron Corporation, India) (Scheme 2).

2.2.1. Characterization of Au NPs

The UV–visible spectra of the Au NPs were recorded using Shimadzu dual-beam spectrophotometer (Shimadzu, UV 2500, Japan) operated at a resolution of 1 nm between 300 and 800 nm in a 10 mm-path-length quartz cuvette. The Au NPs solution was diluted 20 times with deionised water to avoid errors due to high optical density of the solution. FTIR spectra of the Au NPs were recorded using a Shimadzu 8201 PC FTIR spectrometer. The spectral region between 4000 and 400 cm^{-1} was scanned and the KBr disc method was used for recording spectra. Powder XRD patterns of the Au NPs were also recorded by X-ray diffractometer (XPERT-PRO) operated at 40 kV and 30 mA with Cu Kα radiation ($\lambda = 1.54060$ Å). The powder XRD patterns were obtained in the 2θ range of 10 to 80° at a fixed time mode and at room temperature. Atomic force microscopic images of the Au NPs were taken by using Shimadzu SPM 9500-2 J scanning probe microscope and the roughness was also measured. The transmission electron microscopic images were obtained under 200 kV ultra-high resolution transmission electron microscope (JEOL-2010) to visualize the morphology and size of the synthesized Au NPs. The presence of Au NPs and potential other elemental materials in the lyophilized samples was confirmed by Phoenix EDX. Dynamic light scattering was used to determine the particle size distribution of the lyophilized Au NPs. These were dispersed in milli-Q water by ultrasonic process. The distribution of particle size of the synthesized Au NPs was analyzed using Particle Size Analyzer (Malvern Nano ZS, ZETA Sizers Nanoseries).

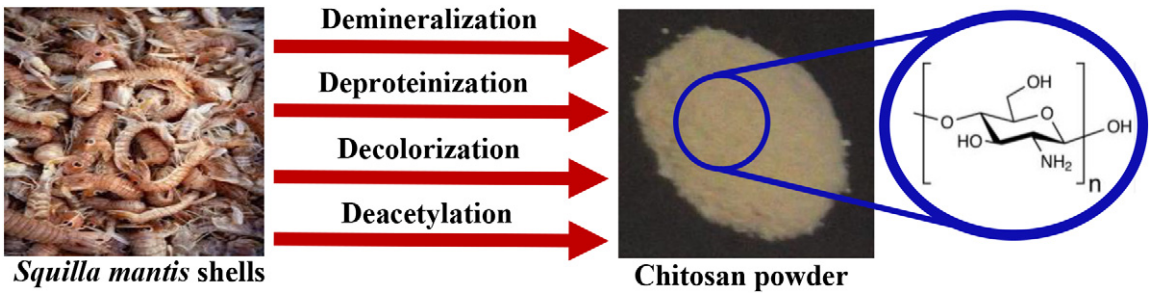

Scheme 1. Schematic representation of chitosan extraction from *Squilla mantis* shell wastes.

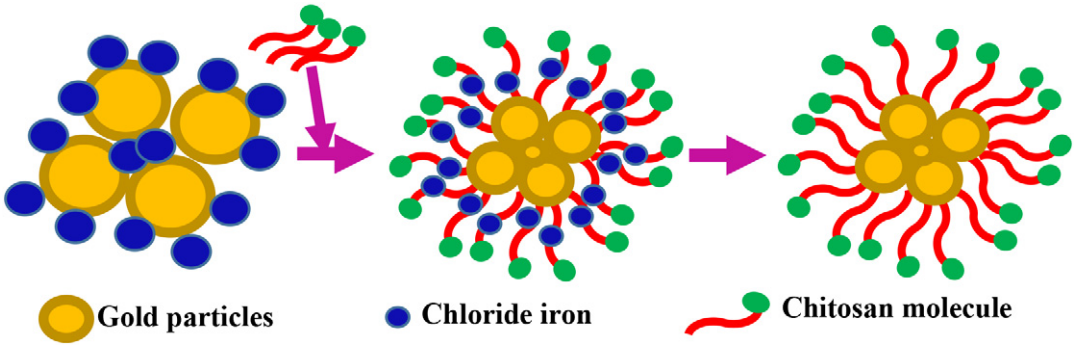

Scheme 2. Schematic illustration of chitosan medicated synthesis of Au NPs.

2.3. Anti-microbial activity of Au NPs

Bacterial cultures such as Staphylococcus sp., and Bacillus sp (gram positive) and *Escherichia coli*, Proteus sp., Pseudomonas sp., Serratia sp. and Klebsiella sp. (gram negative) and fungal cultures such as Aspergillus niger, Aspergillus flavus, Aspergillus fumigatus and *Candida albicans* were collected from Bose clinical laboratory, Madurai, India. Bacteria were cultured in Nutrient Agar (Hi-Media) and the fungi were maintained in Potato Dextrose Agar (PDA).

The agar disc diffusion method was employed to quantify the antibacterial and antifungal activity of the synthesized Au NPs against clinical pathogens. Overnight grown culture (100 μL) of each strain was individually swabbed on a Muller Hinton Agar (MHA) plate. Samples of ~40 μL (100 μg mL^{-1}) of Au NPs were carefully transferred onto sterile discs (6 mm) and placed on MHA plates separately; commercially available ampicillin (25 μg) disc was used as positive control for bacterial cultures. Amphotericin (20 μg) was used as positive control for fungal cultures. The Petri plates were incubated for 24 h at 37 °C for bacteria and 28 °C for 48 h for fungi. After incubation, the zone of inhibition (ZOI) was measured in millimeters. The same experiments were repeated thrice and the mean ± SD are reported.

2.4. Cell lines

The Human breast adenocarcinoma (MCF-7) cell line was procured from the National Centre for Cell Sciences (Pune, India). Cells were grown in T-25 culture flasks containing Dulbecco Modified Eagle's Medium (DMEM) and Roswell Park Memorial Institute (RPMI) – 1640 supplemented with 10% fetal bovine serum (FBS). Upon reaching confluence, the cells were detached using Trypsin Phosphate Versene Glucose (TPVG) solution.

2.4.1. Cell cultivation

Cells were cultured with culture medium in a T-25 tissue culture flask. Cell density was always kept under 2×10^4 cells mL^{-1} to avoid mutations of the cells. Passaging of the cells was done 3 times a week. Cultivation and experimental incubation were performed in a cell incubator at 37 °C, 90% air humidity and 5% CO_2.

2.4.2. MTT assay

The 3-(4, 5-dimethylthiazol-2-yl)-2, 5-diphenyltetrazolium bromide (MTT) dye reduction assay was performed to determine the cytotoxic effect of the Au NPs at various concentrations. The assay depends on the reduction of MTT by mitochondrial succinate dehydrogenase and reductase, an enzyme present in the mitochondria of viable cells, to water insoluble formazan. This blue color product formation is directly proportional to the viable cell number and inversely proportional to the degree of cytotoxicity [37].

The MCF-7 cells were grown in a 96-well plate (ELISA) containing Dulbecco's modified Eagle medium (DMEM) supplemented with 10% heat-inactivated fetal bovine serum and antibiotics. About 1 ml of cell suspension (1×10^5 cells mL^{-1}) was seeded in each well and the cells were cultured in the appropriate medium supplemented with 10% fetal bovine serum and 1% penicillin–streptomycin at 37 °C under 5%

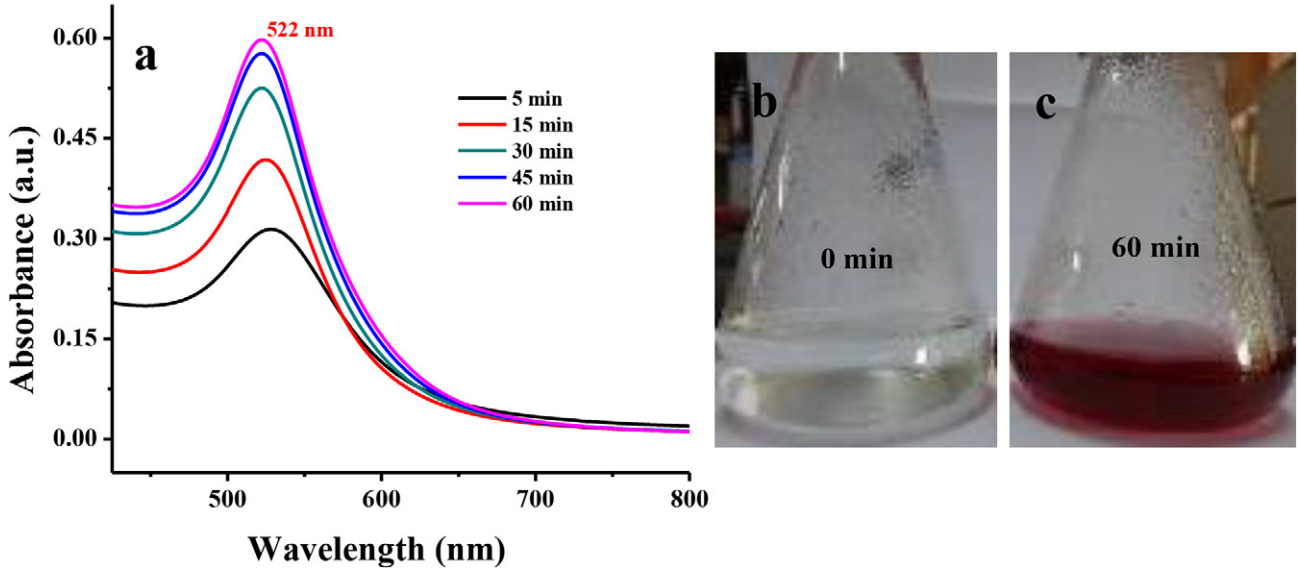

Fig. 1. UV–visible spectrophotometry spectra of chitosan mediated synthesized Au NPs.

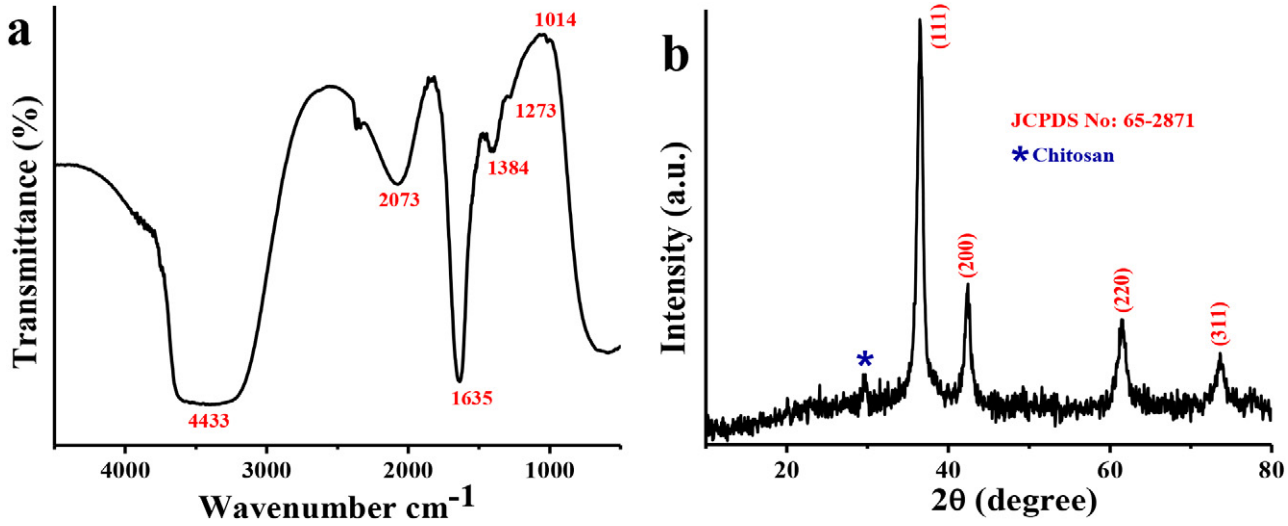

Fig. 2. FTIR spectra showing the wavenumber region from 4500 to 500 cm^{-1} (a), powder XRD pattern in the 2θ range from 20° to 80° of chitosan mediated Au NPs (b).

CO_2 environment for the formation of confluent monolayer. The monolayer of cells in the plate was gently washed with DMEM and exposed to 1 mL of DMEM medium containing different concentration of chitosan mediated synthesized gold NPs (10, 25, 50, 100 and 250 μg mL^{-1}). After 48 h of incubation, 200 μl of MTT (5 mg mL^{-1}) solution and 1 mL of DMSO was added and left for 45 s. The extracted blue MTT formazan was dissolved in 1 mL isopropyl alcohol with the specified percentage of HCl, and their absorbance values were measured at 600 nm using a spectrophotometer (Analytik Jena, Spekol 1200). The untreated cells are used as positive control (i.e., 100% viable), and used for calculating cell viability of treated cells. The results are displayed as percentage of viable cells compared with the control. The

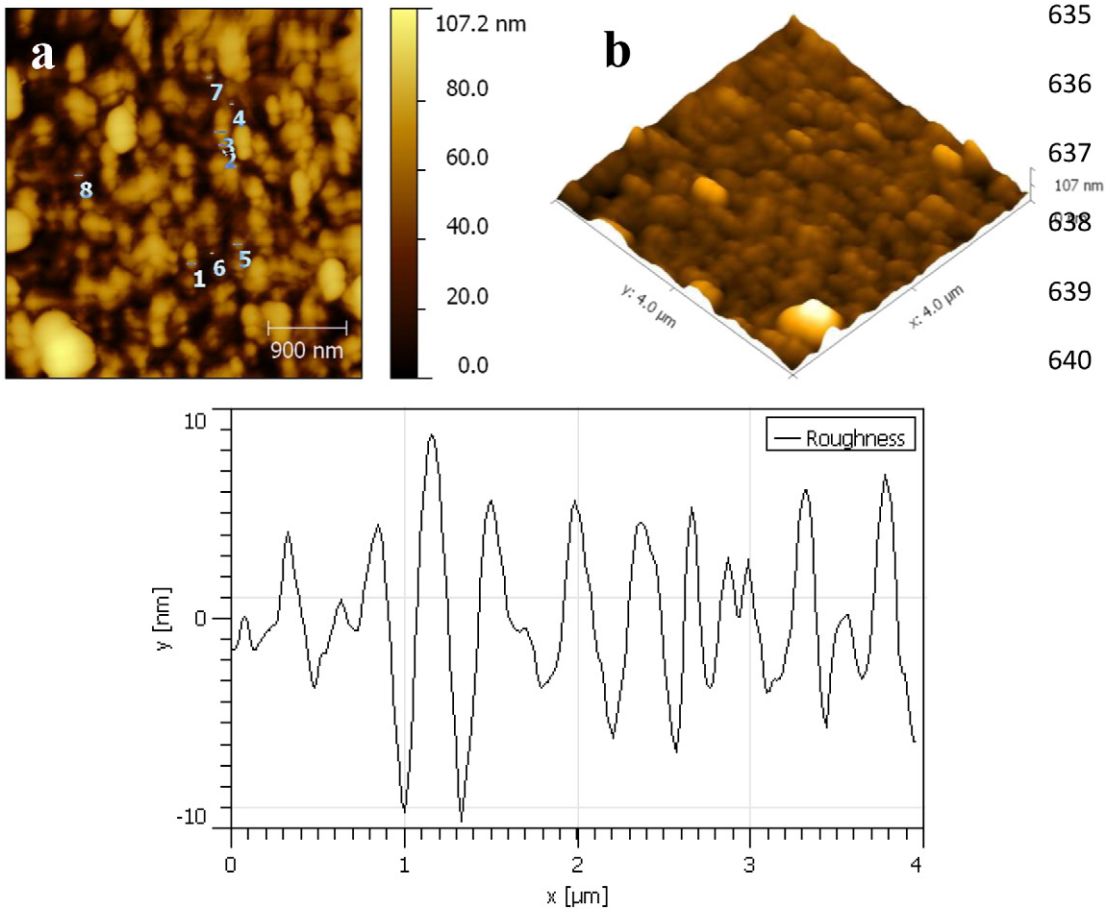

Fig. 3. AFM images obtained in height mode (a), orthogonal projection from height mode (b) and roughness of Ag NPs (c) using morphological identification and surface roughness of chitosan mediated synthesized NPs.

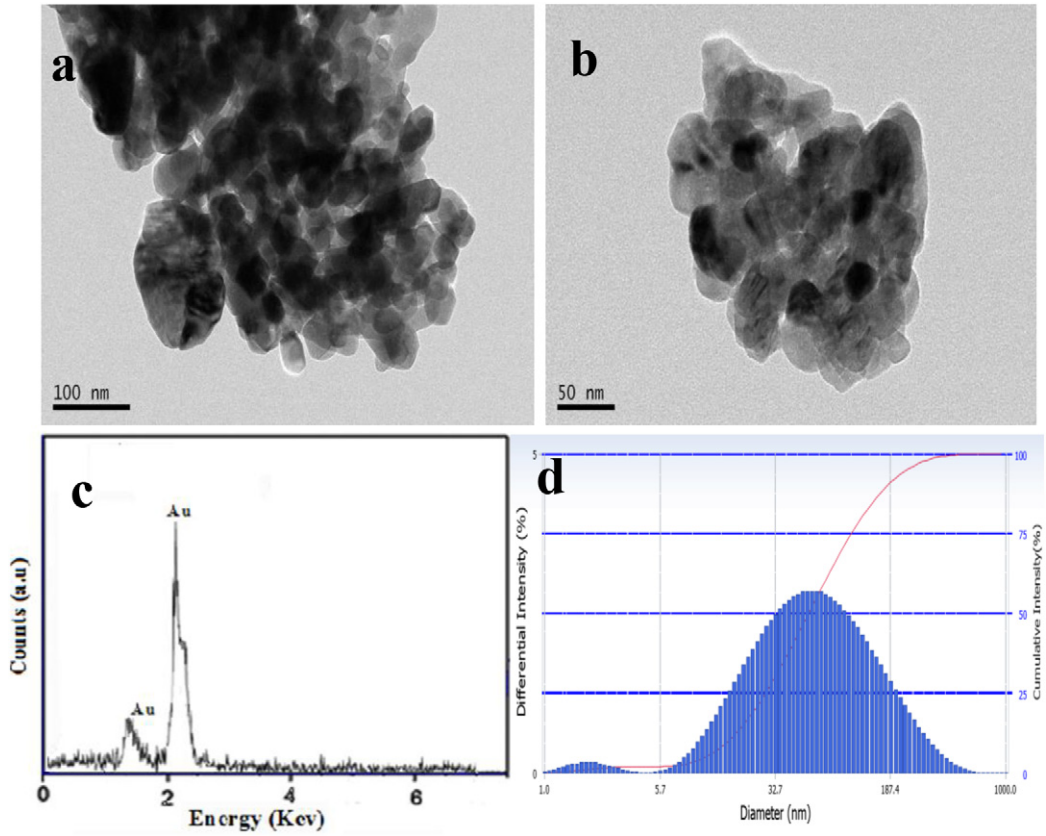

Fig. 4. Low (a) and high (b) magnification TEM images and EDX analysis (c) of Au NPs using atomic percentage of synthesized NPs. DLS analysis of chitosan mediated synthesized Au NPs used to determine their size range and distribution (d).

inhibitory concentration required to inhibit the growth by 50% (IC_{50}) was calculated using Graphpad prism and the equation

$$\text{Cellviability}(\%) = \text{A570 of drug treated sample}/\text{A570 of control} \times 100.$$

2.4.3. Morphological changes

MCF-7 cells were grown and incubated with synthesized Au NPs at different concentrations between 10 and 250 μg/ ml and then they were fixed in methanol: acetic acid (3:1, v/v). The cover slips were gently mounted on glass slides for morphometric analysis. Morphological changes of MCF-7 cells were observed by phase contrast microscopy (Carl Zeiss Inc., Germany).

2.4.4. Acridine orange/ethidium bromide (AO/EB) staining

The AO/EB staining was carried out to find the morphological evidence of apoptosis according to Ribble et al. [38]. The MCF-7 cells were treated with 250 μg/ ml concentration of synthesized Au NPs for about 24 h. Fluorescent dyes, ethidium bromide (100 μg mL^{-1}) and acridine orange (100 μg mL^{-1}) were added to the fixed cells and incubated in dark condition for 10 min at room temperature. Changes in the nuclei of cells were observed within 15 min after AO/EB staining under an Olympus inverted fluorescence microscope (Ti-Eclipse) at 200× and 400× magnifications. The untreated cells were used as

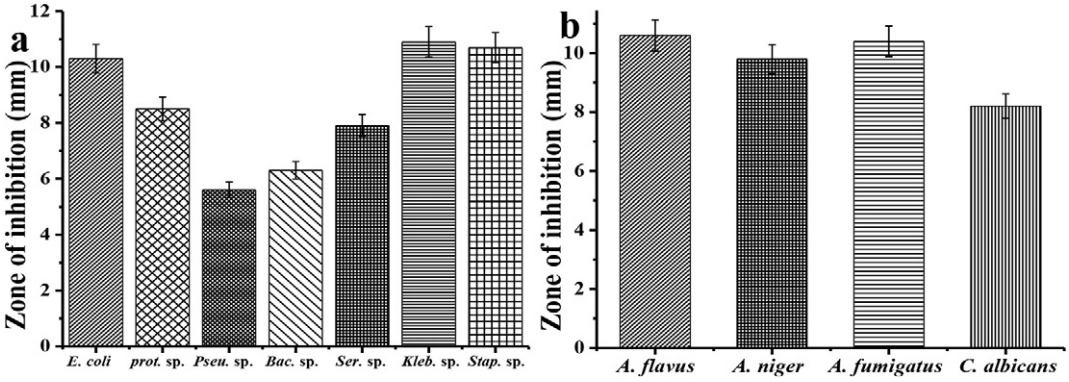

Fig. 5. Antibacterial (a) activity of Au NPs using *Staphylococcus* sp., and *Bacillus* sp., *Escherichia coli*, *Proteus* sp., *Pseudomonas* sp., *Serratia* sp. and *Klebsiella* sp. and antifungal (b) activity of Au NPs using *Aspergillus niger*, *Aspergillus flavus*, *Aspergillus fumigatus* and *Candida albicans*.

Table 1
Antimicrobial activity of Au NPs data with statistical analysis mean ± SD.

Sl. No	Bacterial strains	ZOI Mean ± SD (mm)
1	*E. coli*	10.3 ± 0.51
2	Proteus Sp.	8.5 ± 0.42
3	Pseudomonas Sp.	5.6 ± 0.28
4	Bacillus Sp.	6.3 ± 0.32
5	Serritia Sp.	7.9 ± 0.40
6	Klebsiella Sp.	10.9 ± 0.54
7	Staphylococcus Sp.	10.7 ± 0.54
Sl. No	Fungal strains	ZOI Mean ± SD (mm)
8	*A. flavus*	10.6 ± 0.53
9	*A. niger*	9.8 ± 0.49
10	*A. fumigatus*	10.4 ± 0.52
11	*C. albicans*	8.2 ± 0.41

control. A minimum of 100 cells was counted in each sample. Morphological criteria were used to evaluate cell injury. Cells containing normal nuclear chromatin exhibit green nuclear staining. Cells containing fragmented nuclear chromatin due to apoptosis exhibit yellow to red nuclear.

3. Results and discussion

3.1. Characterization of Au NPs

UV–visible spectroscopy is an important technique to determine the morphology and stability of Au NPs. In the present study, chitosan extracted from *squilla* was mixed with gold chloride and the reaction mixture was monitored every 10 min up to 60 min of incubation. No color change was observed in control, whereas Au NPs synthesis was confirmed by the color change occuring in other samples. The appearance of colorless to ruby red is an indication for the production of Au NPs [39]. The color change in the reaction mixture could be due to the collective oscillation of free electrons present in reduced Au NPs [40]. Fig. 1a shows the UV–visible spectra maximum peaks, occurring due to presence of Au NPs synthesized in the presence of chitosan at different incubation periods. In case of gold ion reduction, the band corresponds to the surface plasmon resonance (SPR) that occurred at 522 nm. The SPR undergoes red shift or blue shift depending on the quantum size effects. Broad peaks are indicative of the polydispersity nature of Au NPs in the solution. It is well known that the optical properties of metal NPs strongly depend on their size and shape. The height of the peak is proportional to the concentration of the Au NPs produced and the shift of the peak towards a lower wavelength depending upon the incubation time indicates the reduction of particle size [41]. In the present study, the intensity of surface plasmon peaks of Au NPs was found maximum at 60 min of incubation period. A color change of Au NPs from colorless to pink color was observed during the synthesis and incubated at 60 min (Fig. 1b,c). This suggests that the reducing and capping abilities of chitosan are realized and are efficient in their function at this gold salt concentration. The technique outlined above proved to be very useful for the analysis of nanoparticles [42].

The FTIR spectrum of the synthesized Au NPs show peaks at wavenumber positions of ~585, 1014, 1273, 1384, 1635, 2073 and 3433 cm^{-1} (Fig. 2a). The intense broad absorbance peak located at ~3433 cm^{-1} is for the hydrogen—bonded O-H stretching. The band located at ~2073 cm^{-1} is related to the stretching vibration of H–bonded alcohols. The band located at ~1635 cm^{-1} denotes the vibration of N—H bending of primary amines. The band located at ~1384 cm^{-1} relates to the N═O bending and the bands located at ~1273 and 1014 cm^{-1} belong to the C—O stretching of alcohols, carboxylic acids, esters and ethers.

The powder XRD pattern of the Au NPs is shown in Fig. 2b. Number of Bragg reflections located at 2θ values of ~37.1, 43.6, 62.9 and 74.1° correspond to the (1 1 1), (2 0 0), (2 2 0) and (3 1 1) Miller indices, respectively. The data indicate that the synthesized Au NPs are spherical in shape and crystalline in nature (ICCD-JCPDS card no. 65-2871), which is in agreement with Karthik et al. [43]. Although the Au NPs are spherical and crystalline in nature, other small peaks possibly related to the presence of bioorganic compounds/proteins, possibly left

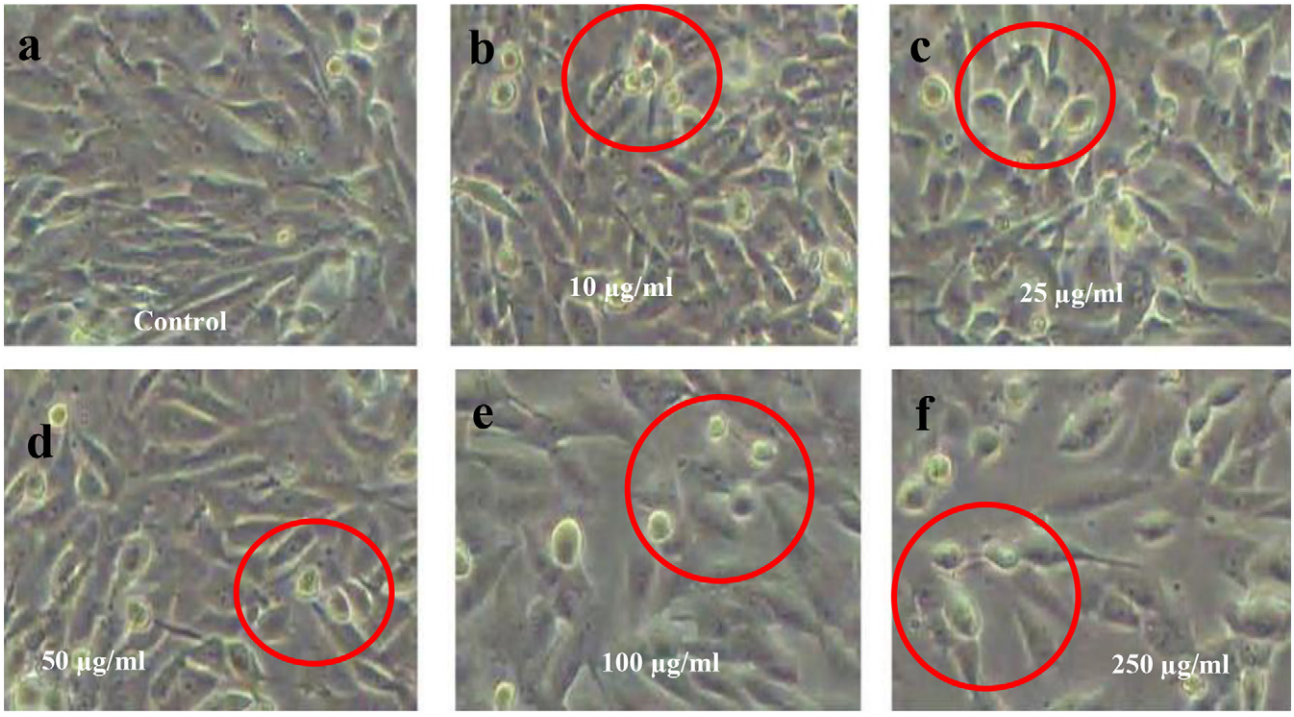

Fig. 6. MCF-7 cells treated with different concentrations of chitosan mediated synthesized Au NPs, control MCF-7 cells not treated with Au NPs (a), MCF-7 cells treated with 10 µg/ml of Au NPs (b), MCF-7 cells treated with 25 µg/ml of Au NPs (c), MCF-7 cells treated with 50 µg/ml of Au NPs (d), MCF-7 cells treated with 100 µg/ml of Au NPs (e) and MCF-7 cells treated with 250 µg/ml of Au NPs (f).

during the removal of impurities, can sometimes be observed [44]. The obtained powder XRD pattern clearly illustrates that the gold ions were reduced to gold NPs and stabilized by the presence of chitosan. The powder XRD pattern shows the reflection planes that confirm the presence face-centered cubic form of metallic gold and no peaks of other impurity crystalline phases were observed [45].

The AFM images depict the surface morphology and size of the synthesized Au NPs. The images revealed that the synthesized Au NPs are spherical without other observable nanostructure morphologies, as suggested by the UV–visible absorbance spectrum. Furthermore, the particles are polydispersed, without agglomeration occurring between them (Fig. 3a,b). The particles are not monodispersed and non-agglomerated since the presence of some essential bio organic compounds present in the chitosan possibly act as ligand and stabilize the synthesized Au NPs. The size of the synthesized Au NPs is ~80 nm. AFM images show the spherical shape of the Au NPs with an average diameter of 85 nm. Additionally, the Au NPs surface appeared regular without roughness. The lack of pores at the surface of Au NPs as suggested by AFM imaging is due to that the cavities are smaller than the AFM tips (about 1 nm). Generally, the particles appear well separated on glass slide, indicating that the surface-capping agents prevent aggregation of NPs. The roughness of the Au NPs was measured by AFM. Maximum roughness (R_p) peak height value of 8.9 nm, average maximum roughness (R_{pm}) peak height value of 6.1 nm, maximum roughness valley depth (R_v) value of 7.4 nm and average maximum roughness valley depth (R_{vm}) value of 5.9 nm for the chitosan mediated synthesized Au NPs were obtained (Fig. 3c).

The morphology, size distribution and chemical composition of the Au NPs were examined by TEM (Fig. 4a,b) coupled with energy-dispersive X-ray spectroscopy (EDX) (Fig. 4c). EDX analysis of the Au NPs shows strong signals for gold along with other weak signals. These weak signals could come from chitosan macromolecules present at the surface of Au NPs acting as capping agents. Fig. 4c shows two strong signals for Au NPs at different energy positions and confirms the presence of gold as Au NPs [46]. In addition, a considerable peak is also observed in Au NPs specific site. The image shows that Au NPs were spherical and polydispersed with their size ranging from 80 up to 83 nm. The results observed using UV–visible spectrophotometry, powder XRD, AFM, and TEM was further supported by DLS. The aqueous dispersion of chitosan mediated Au NPs was analyzed by DLS at 25 °C. The result of the DLS shows that 53% of the nanoparticles were 5 nm in size and 37% of nanoparticles were 10 nm in size (Fig. 4d). The average size distribution of Au NPs in aqueous solution was found to be 82.7 nm.

3.2. Antimicrobial activity

The antibacterial and anti-fungal activity of Au NPs against clinical pathogens were investigated. The inhibition of microbial growth around the disc is due to the release of diffusible inhibitory compounds that originate from Au NPs. The Au NPs show the potential inhibitory activity against *E.coli*, *Staphylococcus sp*, *Klebsiella sp* with the ZOI of 13, 10 and 12 mm, respectively. The ZOI of *Serratia sp* and *Proteuss sp* were 8 mm (Fig. 5a). The Au NPs show the least antibacterial activity against other bacterial isolates such as *Pseudomonas sp* and *Bacillus sp* (Table 1). Prema and Thangapandiyan [47] reported antibacterial activity of Au NPs with and without chitosan capping agent. The Au NPs elicit antibacterial activity either by generating holes and pits on the cell wall due to surface ionization that affects the membrane permeability, resulting in leakage of the cell contents. The Au NPs bind to the bacterial DNA and inhibit the unwinding and transcription process [48,49]. The synthesized Au NPs are more active against gram-negative than positive bacteria. The difference in the antibacterial activity may be related to the cell wall compositions of these bacteria. The outer membrane of gram-negative cells is more complex and contains specialized protein and polysaccharides. These proteins are involved in membrane permeability and intrude with the entry of Au NPs and cause slow or prevent the entry into the cell [50]. On the other hand, the cell wall of gram-positive bacteria does not contain the special layers that possess gram-negative bacteria and allows the Au NPs entering the cell membrane. The Au NPs alters the membrane potential, affect ATP synthesis enzyme activities and reduce the ATP level, representing a wide-range decline in metabolism; moreover it inhibits the tRNA binding with the subunit of ribosome and significantly affects the biological process [51,52].

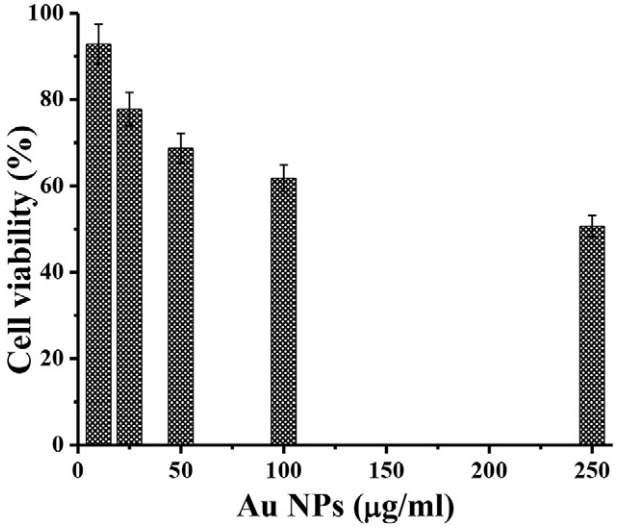

Fig. 7. Cell viability of chitosan mediated synthesized Au NPs treated MCF-7 cells with different concentration of Au NPs (10 μg/ml – 250 μg/ml).

The synthesized Au NPs show activity against *A. niger* (13 mm), *A. fumicatus* (10 mm) *Aspergillus flavus* (11 mm) and for *Candida albicans* (12 mm) (Fig. 5b). The synthesized Au NPs are highly active against *A. niger* compared to the other fungal isolates (Table 1). The Au NPs interact with fungal membrane proteins and alter their normal conformations, leading to the loss of their activity. Thus, fungal membrane is incapable of regulating the H^+ transport across the membrane, leading to the retardation of the cell growth. This finally causes the cell death [53]. In a previous study, it was shown that the antifungal activity of Au NPs is size dependent. The extent of inhibition increased upon decreasing particle size [54]. In this study, Au NPs with 2–10 nm size were active against *Aspergillus* sp. and *Candida* sp. This may be due to the fact that decrease in the particle size increases the surface area of the Au NPs, which enhances its interaction with the binding sites of the plasma membrane proteins. Furthermore, it may be assumed that the smaller Au NPs may diffuse easily through the cell membrane and reach the core of fungal cell. Since gold has greater tendency to react with the sulphur and phosphorus containing soft bases, the synthesized NPs interact with the sulphur containing proteins in the membrane or the phosphorus containing bases in the DNA of the cells to retard their normal functioning like replication, synthesis, repair, which leads finally to the cell death [55].

3.3. Anticancer activity

The MCF-7 cancer cells were exposed to Au NPs at various concentrations like 10, 25, 50, 100 and 250 μg mL^{-1}. The result shows that

Table 2
Cell viability of MCF-7 cell lines against chitosan mediated synthesized Au NPs.

Au NPs (μg ml^{-1})	Cell viability (%)	
10	92.83 ± 7	IC_{50}–230.2 μg ml^{-1}
25	77.75 ± 1.25	
50	68.75 ± 5.92	
100	61.83 ± 3	
250	50.67 ± 0.5	

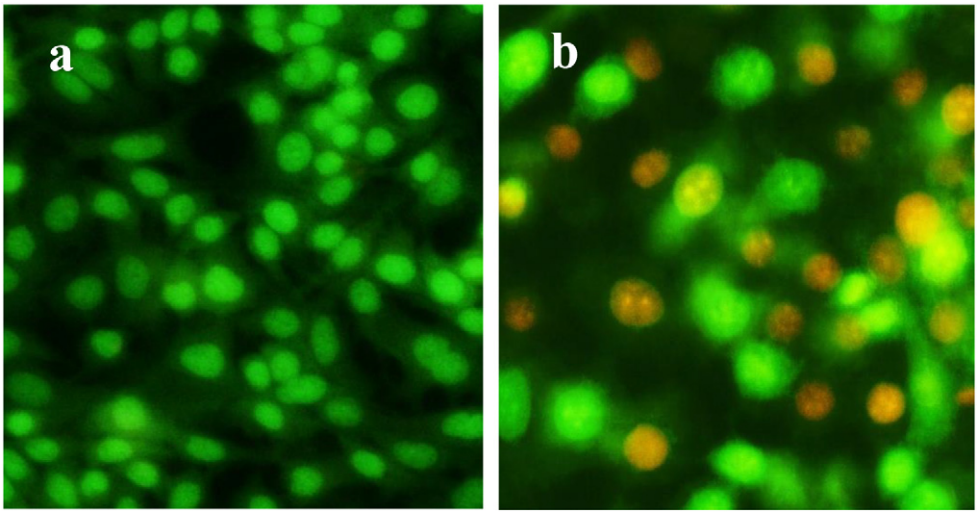

Fig. 8. Live/death cells images obtained after AO/EB staining of MCF-7 control cells (a), MCF-7 cells treated with *squilla* chitosan mediated Au NPs (b).

the percentage of cell viability gradually decreased upon increasing concentration of Au NPs (Table 1), suggesting a dose dependent behaviour. Furthermore, the highest cell viability was observed for cells treated with the lowest concentration of Au NPs. The Au NPs show enhanced activity in all the tested concentrations except at 25 μg mL^{-1}. This suggests that the Au NPs possess better inhibition ability even at relatively low concentration. Likewise, the study of Martínez-Torres et al. [56] showed the IC_{50} of chitosan Au NPs was 75 μM against MCF 7 and cell lines. Furthermore, it is debated that the effect of Au NPs against cancer cells is size, shape and surface charge dependent and that the higher the positivity, the greater the effect [57].

The changes in morphology of cells treated with Au NPs were analyzed by inverted phase contrast light microscopy. The results revealed that the control MCF-7 cells showed characteristic including spindle shape morphology, resembling healthy fibroblasts (Fig. 6a).On the other hand, the MCF-7 cells treated with different concentrations of Au NPs showed distorted morphology resembling dead fibroblasts (Fig. 6a–f). This is represented graphically in Fig. 7. The IC_{50} value of 230.2 μg mL^{-1} was observed for Au NPs against MCF-7 cell line (Table 2).

To find whether the cytotoxic effect of NPs can be related to the induction of apoptosis, morphological assay of dead cells was investigated by using AO/EB double staining and subsequently visualized under fluorescence microscopy. As shown in Fig. 8a, no obvious morphological changes were observed in the control and almost all the cells were stained green, indicating the viability (~100%) of the control cells. On the contrary, the cells (treated with 230.2 μg mL^{-1}) at early apoptosis stage were visualized as green arcs and the cells at late apoptotic stage were observed as yellow/orange nuclei. This observation suggested that the cells exposed to chitosan-mediated synthesized Au NPs induce apoptosis in MCF cell lines and inhibit the proliferations of MCF cells. Programed cell death or apoptosis is often considered as a mode of action of NPs and other polysaccharides. Apoptosis may occur either by cell shrinkage or DNA fragmentation [58]. In the present study, we observed the characteristic features of apoptotic cells such as condensed nuclei and apoptotic bodies (Fig. 8b) when the cells are treated with chitosan-mediated synthesized Au NPs. The chitosan-mediated synthesized Au NPs cell death in MCF cells is not depend on caspase activity [56] but depends on ROS production. Furthermore, Martínez-Torres et al. [56] showed that the chitosan-mediated synthesized Au NPs did not induce nuclear alterations in MCF cells and did not modify the cell cycle. Also, they were found to inhibit the long-term proliferations of cancer cells. In addition, the mechanism of cell death of Au NPs depends on the materials used for NP synthesis as well as the cell lines used. Hence, it can be concluded that the chitosan-mediated synthesized Au NPs induce ROS mediated cell death.

4. Conclusion

The present study summarizes the facile synthesis of Au NPs using *squilla* shell chitosan as a template. The adopted method is compatible with green chemistry principle as the chitosan biopolymer can improve the reduction and stability of Au NPs. The use of biopolymers in the synthesis of nanoparticles in nanotechnology enables environmentally friendly, easily scaled up for large-scale synthesis. The proposed methodology is free of using high pressure, energy, temperature and toxic chemicals. The formation, size, shape and elemental composition of the synthesized Au NPs was confirmed by UV–visible spectrophotometry, FTIR spectroscopy, powder XRD, AFM, TEM and DLS. The green synthesized Au NPs showed significant antimicrobial action against several pathogenic bacteria and fungi. The in-vitro anticancer activity studied against MCF-7cells showed great activity that would pave the way to further study the activity of the Au NPs against various cancer cell lines. The improper disposal of seafood waste is a continuous problem along the coastal areas. Therefore, our observations indicate the utilization of *squilla* shell waste for high value applications to solve environmental issues and suggest a new platform for nanomedicine preparation and may promote the socioeconomic value of coastal area for local people.

CRediT authorship contribution statement

R. Kalaivani: Investigation, Writing - review & editing. **M. Maruthupandy:** Investigation, Writing - original draft, Writing - review & editing. **T. Muneeswaran:** Investigation. **Manoj Singh:** Writing - review & editing. **S. Sureshkumar:** Formal analysis, Writing - review & editing. **M. Anand:** Writing - original draft, Writing - review & editing. **C.M. Ramakritinan:** Writing - original draft, Writing - review & editing. **F. Quero:**Writing - original draft, Writing - review & editing. **A.K. Kumaraguru:** Writing - original draft, Writing - review & editing.

Acknowledgement

The authors are grateful to University Grants Commission India, New Delhi for financial assistance for this study (F.No.39-559/2010 (SR) and dt 12.01.2011). The authors express their thanks to the University with Potential for Excellence (UPE) Scheme, Madurai Kamaraj University, for generously providing instruments facility. Acknowledgement is

extended to Pondicherry Centre for Biological Sciences, Puducherry for their support in performing cell line studies.

References

[1] N.K. Kaushik, N. Kaushik, N.N. Linh, B. Ghimire, A. Pengkit, J. Sornsakdanuphap, S.-J. Lee, E.H. Choi, Plasma and nanomaterials: fabrication and biomedical applications, Nanomaterials (Basel) 9 (2019) 98.

[2] Z.T. Luo, K.Y. Zheng, J.P. Xie, Engineering ultrasmall water-soluble gold and silver nanoclusters for biomedical applications, Chem. Commun. 50 (2014) 5143–5155.

[3] E.C. Dreaden, A.M. Alkilany, X.H. Huang, C.J. Murphy, M.A. El-Sayed, The golden age: gold nanoparticles for biomedicine, Chem. Soc. Rev. 41 (2012) 2740–2779.

[4] R. Levy, N.T.K. Thanh, R.C. Doty, I. Hussain, R.J. Nichols, D.J. Schiffrin, et al., Rational and combinatorial design of peptide capping ligands for gold nanoparticles, J. Am. Chem. Soc. 126 (2004) 10076–10084.

[5] S. Govindaraju, S.R. Ankireddy, B. Viswanath, J. Kim, K. Yun, Fluorescent gold nanoclusters for selective detection of dopamine in cerebrospinal fluid, Sci. Rep. 7 (2017), 40298. https://doi.org/10.1038/srep40298.

[6] R.R. Arvizo, S. Bhattacharyya, R. Kudgus, K. Giri, R. Bhattacharya, P. Mukherjee, Intrinsic therapeutic applications of noble metal nanoparticles: past, present and future, Chem. Soc. Rev. 41 (2012) 2943–2970.

[7] P.R. Rauta, P.M. Hallur, A. Chaubey, Gold nanoparticle-based rapid detection and isolation of cells using ligand-receptor chemistry, Sci. Rep. 8 (2018) 2893.

[8] P. Singh, S. Pandit, V.R.S.S. Mokkapati, A. Garg, V. Ravikumar, I. Mijakovic, Gold nanoparticles in diagnostics and therapeutics for human cancer, Int. J. Mol. Sci. 19 (2018) 1979.

[9] A. Banerjee, T. Pons, N. Lequeux, B. Dubertret, Quantum dots–DNA bioconjugates: synthesis to applications, Interface Focus 6 (2016), 20160064.

[10] M. Gholipourmalekabadi, M. Mobaraki, M. Ghaffari, A. Zarebkohan, V.F. Omrani, A.M. Urbanska, A. Seifalian, Targeted drug delivery based on gold nanoparticle derivatives, Curr. Pharm. Des. 23 (2017) 2918–2929.

[11] H. Katasa, C.S. Lima, A.Y.H.N. Azlana, F. Buanga, M.F.M. Busra, Antibacterial activity of biosynthesized gold nanoparticles using biomolecules from *Lignosus rhinocerotis* and chitosan, Saudi Pharm. J. 27 (2019) 283–292.

[12] F. Foglietta, G.C. Spagnoli, M.G. Muraro, M. Ballestri, A. Guerrini, C. Ferroni, A. Aluigi, G. Sotgiu, G. Varchi, Anticancer activity of paclitaxel-loaded keratin nanoparticles in two-dimensional and perfused three-dimensional breast cancer models, Int. J. Nanomedicine 13 (2018) 4847–4867.

[13] M.U. Farooq, V. Novosad, E.A. Rozhkova, H. Wali, A. Ali, A.A. Fateh, P.B. Neogi, A. Neogi, Z. Wang, Gold nanoparticles-enabled efficient dual delivery of anticancer therapeutics to hela cells, Sci. Rep. 8 (2018) 2907.

[14] Y. Ishida, I. Akita, T. Sumi, M. Matsubara, T. Yonezawa, Thiolate–protected gold nanoparticles via physical approach: unusual structural and photophysical characteristics, Sci. Rep. 6 (2016), 29928.

[15] L.F. Freitas, G.H.C. Varca, J.G.S. Batista, A.B. Lugão, An overview of the synthesis of gold nanoparticles using radiation technologies, Nanomaterials (Basel) 8 (2018) 939.

[16] J.C. Scaiano, K.G. Stamplecoskie, G.L. Hallett-Tapley, Photochemical norrish type I reaction as a tool for metal nanoparticle synthesis: importance of proton coupled electron transfer, Chem. Commun. 48 (2012) 4798–4808.

[17] A. Lassenberger, T.A. Grünewald, P.D.J. van Oostrum, H. Rennhofer, H. Amenitsch, R. Zirbs, H.C. Lichtenegger, E. Reimhult, Monodisperse iron oxide nanoparticles by thermal decomposition: elucidating particle formation by second-resolved in situ small-angle x-ray scattering, Chem. Mater. 29 (2017) 4511–4522.

[18] K. Richter, A. Birkner, A.-V. Mudring, Stability and growth behavior of transition metal nanoparticles in ionic liquids prepared by thermal evaporation: how stable are they really? Phys. Chem. Chem. Phys. 13 (2011) 7136–7141.

[19] T.L. Botha, E.E. Elemike, S. Horn, D.C. Onwudiwe, J.P. Giesy, V. Wepener, Cytotoxicity of Ag, Au and Ag-Au bimetallic nanoparticles prepared using golden rod (*Solidago canadensis*) plant extract, Sci. Rep. 9 (2019) 4169.

[20] J. Singh, T. Dutta, K.-H. Kim, M. Rawat, P. Samddar, P. Kumar, Green synthesis of metals and their oxide nanoparticles: applications for environmental remediation, J Nanobiotechnol 16 (2018) 84.

[21] E.C. Wang, A.Z. Wang, Nanoparticles and their applications in cell and molecular biology, Integr. Biol. (Camb) 6 (2014) 9–26.

[22] P. Velusamy, G.V. Kumar, V. Jeyanthi, J. Das, R. Pachaiappan, Bio-inspired green nanoparticles: synthesis, mechanism, and antibacterial application, Toxicol. Res. 32 (2016) 95–102.

[23] J. Jeevanandam, A. Barhoum, Y.S. Chan, A. Dufresne, M.K. Danquah, Review on nanoparticles and nanostructured materials: history, sources, toxicity and regulations, Beilstein J. Nanotechnol. 9 (2018) 1050–1074.

[24] I. Younes, M. Rinaudo, Chitin and chitosan preparation from marine sources structure, properties and applications, Mar. Drugs 13 (2015) 1133–1174.

[25] D. Moura, J.F. Mano, M.C. Paiva, N.M. Alves, Chitosan nanocomposites based on distinct inorganic fillers for biomedical applications, Sci. Technol. Adv. Mater. 17 (2016) 626–643.

[26] S.A. Dahoumane, C. Jeffryes, M. Mechouet, S.N. Agathos, Biosynthesis of inorganic nanoparticles: a fresh look at the control of shape, size and composition, Bioengineering (Basel) 4 (2017) 14.

[27] A. Mohandas, S. Deepthi, R. Biswas, R. Jayakumar, Chitosan based metallic nanocomposite scaffolds as antimicrobial wound dressings, Bioact. Mater. 3 (2018) 267–277.

[28] A. Valdés, A.C. Mellinas, M. Ramos, M.C. Garrigós, A. Jiménez, Natural additives and agricultural wastes in biopolymer formulations for food packaging, Front. Chem. 2 (2014) 6.

[29] A. Aravamudhan, D.M. Ramos, A.A. Nada, S.G. Kumbar, Chapter 4 - natural polymers: polysaccharides and their derivatives for biomedical applications, Natural and Synthetic Biomedical Polymers 67 (2014) 67–89.

[30] B. Jia, Y. Mei, L. Cheng, J. Zhou, L. Zhang, Preparation of copper nanoparticles coated cellulose films with antibacterial properties through one-step reduction, ACS Appl. Mater. Interfaces 4 (2012) 2897–2902.

[31] K. Wongmanee, S. Khuanamkam, S. Chairam, Gold nanoparticles stabilized by starch polymer and their use as catalyst in homocoupling of phenylboronic acid, JKSUS 29 (2017) 547–552.

[32] S. Deguchi, K. Tsujii, K. Horikoshi, In situ microscopic observation of chitin and fungal cells with chitinous cell walls in hydrothermal conditions, Sci. Rep. 5 (2015), 11907.

[33] M. Anand, R. Kalaivani, M. Maruthupandy, A.K. Kumaraguru, S. Suresh, Extraction and characterization of chitosan from marine crab and squilla collected from the gulf of Mannar region, South India, J. Chitin and Chitosan Sci. 2 (2014) 280–287.

[34] S. Kumar, S.R. Smith, G. Fowler, C. Velis, S. Jyoti Kumar, S. Arya, Rena, R. Kumar, C. Cheeseman, Challenges and opportunities associated with waste management in India, R. Soc. Open Sci. 4 (2017), 160764.

[35] M. Anand, M. Maruthupandy, R. Kalaivani, S. Suresh, A.K. Kumaraguru, Larvicidal activity of chitosan nanoparticles synthesized from crab and squilla species against *Aedes aegypti*, J. Colloid Sci. Biotechnol. 3 (2014) 188–193.

[36] H.Z. Huang, X.R. Yang, Synthesis of chitosan-stabilized gold nanoparticles in the absence/presence of tripolyphosphate, Biomacromolecules 9 (2004) 2340–2346.

[37] T. Mosmann, Rapid colorimetric assay for cellular growth and survival: application to proliferation and cytotoxicity assays, J. Immunol. Methods 16 (1983) 55–63.

[38] D. Ribble, N.B. Goldstein, D.A. Norris, Y.G. Shellman, A simple technique for quantifying apoptosis in 96-well plates, BMC Biotechnol. 10 (2005) 12.

[39] B.S. Srinath, R.V. Rai, Biosynthesis of gold nanoparticles using extracellular molecules produced by enterobacter aerogenes and their catalytic study, J. Clust. Sci. (2015) https://doi.org/10.1007/s10876-014-0835-9.

[40] M.A. Noginov, G. Zhu, M. Bahoura, J. Adegoke, C. Small, B.A. Ritzo, V.P. Drachev, V.M. Shalaev, The effect of gain and absorption on surface plasmos in metal nanoparticles, Appl. Phys. B Lasers Opt. 86 (2006) 455–460.

[41] S.A. Aromal, K.V. Babu, D. Philip, Characterization and catalytic activity of gold nanoparticles synthesized using ayurvedic arishtams, Spectrochim. Acta A Mol. Biomol. Spectrosc. 96 (2012) 1025–1030.

[42] J.N. Thakker, P. Dalwadi, P.C. Dhandhukia, Biosynthesis of gold nanoparticles using *Fusarium oxysporum* f. sp. cubense JT1, a plant pathogenic fungus, ISRN Biotechnol 2013 (2013), 515091.

[43] L. Karthik, G. Kumar, T. Keswani, A. Bhattacharyya, B.A. Reddy, K.V.B. Rao, Marine actinobacterial mediated gold nanoparticles synthesis and their antimalarial activity, Nanomedicine Nanotechnol. Biol. Med. 9 (2013) 951–960.

[44] S.S. Shankar, A. Rai, A. Ahmad, M. Sastry, Rapid synthesis of Au, Ag, and bimetallic Au core-Ag shell nanoparticles using Neem (*Azadirachta indica*) leaf broth, J. Colloid Interface Sci. 275 (2004) 496–502.

[45] M. Yang, X. Yang, L. Huai, Synthesis and characterizations of hollow spheres and nanospheres of Au, Applied Physics A 92 (2008) 367–370.

[46] S. Gurunathan, J.-H. Kim, Biocompatible gold nanoparticles ameliorate retinoic acid-induced cell death and induce differentiation in F9 teratocarcinoma stem cells, Nanomaterials (Basel) 8 (2018) 396.

[47] P. Prema, S. Thangapandiyan, In-vitro antibacterial activity of gold nanoparticles capped with polysaccharide stabilizing agents, Int. J. Pharmacy and Pharmaceutical Sciences 5 (2013) 310–314.

[48] P. Singh, A. Garg, S. Pandit, V.R.S.S. Mokkapati, I. Mijakovic, Antimicrobial effects of biogenic nanoparticles, Nanomaterials 8 (2018) 1009.

[49] J.M. Kaguni, A. Dna, A controlling the initiation of bacterial DNA replication and more, Annu. Rev. Microbiol. 60 (2006) 351–375.

[50] Y. Cui, Y. Zhao, Y. Tian, W. Zhang, X. Lü, X. Jiang, The molecular mechanism of action of bactericidal gold nanoparticles on *Escherichia coli*, Biomaterials 33 (2012) 2323–2333.

[51] Y. Kagawa, ATP synthase: from single molecule to human bioenergetics, Proc. Jpn. Acad. Ser. B Phys. Biol. Sci. 86 (2010) 667–693.

[52] Y. Zhao, Y. Tian, Y. Cui, W. Liu, W. Ma, X. Jiang, Small molecule-capped gold nanoparticles as potent antibacterial agents that target Gram-negative bacteria, J. Amer. Chem. Soc. 132 (2010) 12349–12356.

[53] E. Ben-Josef, J. Moughan, J.A. Ajani, M. Flam, L. Gunderson, J.D. Pollock, R. Myerson, R. Anne, S.A. Rosenthal, C. Willett, Impact of overall treatment time on survival and local control in patients with anal cancer: a pooled data analysis of radiation therapy oncology group trials 87-04 and 98-11, J. Clin. Oncol. 28 (2010) 5061–5066.

[54] K.W. Beyenbach, H. Wieczorek, The V-type H+ ATPase: molecular structure and function, physiological roles and regulation, J. Exp. Biol. 209 (2006) 577–589.

[55] M. Tan, H. Luo, S. Lee, F. Jin, J.S. Yang, E. Montellier, T. Buchou, Z. Cheng, S. Rousseaux, N. Rajagopal, Z. Lu, Z. Ye, Q. Zhu, J. Wysocka, Y. Ye, S. Khochbin, B. Ren, Y. Zhao, Identification of 67 histone marks and histone lysine crotonylation as a new type of histone modification, Cell 146 (2011) 1016–1028.

[56] A.C. Martínez-Torres, D.G. Zarate-Triviño, H.Y. Lorenzo-Anota, A. Ávila-Ávila, C. Rodríguez-Abrego, C. Rodríguez-Padilla, Chitosan gold nanoparticles induce cell death in hela and McF-7 cells through reactive oxygen species production, Int. J. Nanomedicine 13 (2018) 3235.

[57] C.M. Goodman, C.D. Mccusker, T. Yilmaz, V.M. Rotello, Toxicity of gold nanoparticles functionalized with cationic and anionic side chains, Bioconjug. Chem. 15 (2004) 897–900.

[58] C. Krishnaraj, P. Muthukumaran, R. Ramachandran, M.D. Balakumaran, P.T. Kalaichelvan, *Acalypha indica* Linn: biogenic synthesis of silver and gold nanoparticles and their cytotoxic effects against MDA-MB-231, human breast cancer cells, Biotechnol. Rep. 4 (2014) 42–49.